energies

MDPI

Article

Heterogeneity and Sedimentary Characteristics of Shale Laminae of Fine-Grained Sediments in Alkaline Lacustrine Strata in the Permian Fengcheng Formation, Mahu Sag, NW China

Mengying Li [1], Songtao Wu [2,*], Rukai Zhu [2], Suyun Hu [2], Pengwan Wang [1], Yi Cai [2] and Surong Zhang [2]

[1] PetroChina Hangzhou Institute of Petroleum Geology, Hangzhou 310023, China; limy0301@163.com (M.L.); wangpw_hz@petrochina.com.cn (P.W.)
[2] Research Institute of Petroleum Exploration and Development (RIPED), China National Petroleum Corporation (CNPC), Beijing 100083, China; zrk@petrochina.com.cn (R.Z.); husy@petrochina.com.cn (S.H.); caiyi813@petrochina.com.cn (Y.C.); zsr_win2019@163.com (S.Z.)
* Correspondence: wust@petrochina.com.cn

Abstract: The heterogeneity, sedimentary characteristics, and distribution of fine-grained sediments of millimeter-scale laminae were studied in alkaline lacustrine strata in the lower Permian Fengcheng Formation (P_1f_2) in the Mahu Sag to provide a sound theoretical basis for shale oil exploration and development. They were investigated by using core and thin-section observation, geochemical and elemental analysis, mineral identification, and pore examination. Five types of laminae were distinguished, with different mineral compositions, pore characteristics, and distributions. These laminae occur in four distinct combinations. The pore systems predominantly consist of intercrystalline pores, intragranular pores, and dissolution pores of feldspar and dolomite and also contain imporous alkaline mineral particles. Influenced by variations in salinity, the influx of volcanic–hydrothermal material, and the participation of both endogenous and exogenous materials, the formation has gone through five stages of sedimentary evolution. Furthermore, felsic laminae (FQL), dolomite laminae (DOL)/reedmergnerite laminae (RL)/shortite laminae (SL), and chert laminae (CL) developed in single-terrestrial-source still water deposition, hybrid-source still water deposition, and single-intrasource deposition, respectively. Vertically, the FQL-DOL combination shows favorable reservoir characteristics and is the most extensively developed lamina combination in the Fengcheng Formation that primarily developed in the period of the late Feng 1 Member (P_1f_1), the early Feng 2 Member (P_1f_2), the late Feng 2 Member (P_1f_2), and the early Feng 3 Member (P_1f_3). The FQL-RL/SL combination primarily developed in the period of the middle P_1f_2, and the DOL-CL combination is the counterpart in the period of the early P_1f_2 and the late P_1f_2 stages. Considering this in conjunction with the longitudinal distribution of lamina combinations, a model is proposed for the distribution of fine-grained sediments in alkaline lacustrine strata.

Keywords: unconventional petroleum accumulation; nanopores; sedimentary evolution; fine-grained sediments; Mahu Sag; Junggar Basin; China

Citation: Li, M.; Wu, S.; Zhu, R.; Hu, S.; Wang, P.; Cai, Y.; Zhang, S. Heterogeneity and Sedimentary Characteristics of Shale Laminae of Fine-Grained Sediments in Alkaline Lacustrine Strata in the Permian Fengcheng Formation, Mahu Sag, NW China. *Energies* **2024**, *17*, 962. https://doi.org/10.3390/en17040962

Received: 28 January 2024
Revised: 16 February 2024
Accepted: 17 February 2024
Published: 19 February 2024

1. Introduction

Shale oil in China is predominantly found in continental facies, characterized by source–reservoir integration and low porosity and permeability. The quality of shale reservoirs is the key to shale oil exploration and development [1–4]. The development of laminae and lamina combinations controls the material composition, geochemical characteristics, pore characteristics, and microfracture distribution of shale reservoirs, which in turn directly affects the reservoir characteristics and oil-bearing properties as well as the mobility of shale oil [5,6]. The study of the different types of shale laminae and their various combinations is therefore of great significance for the evaluation of shale reservoirs and the identification of exploration sweet spots.

The Fengcheng Formation in the Mahu Sag, Junggar Basin, is the oldest alkaline lacustrine sedimentary deposit so far discovered in China. Its discovery drew widespread attention and, in the past decade, its high-quality source rocks have supported the development of the billion-ton Mahu oil field. The Fengcheng Formation is a rare hybrid of sedimentary deposits with alkaline minerals, deposited in an evaporative volcanic–alkaline lacustrine environment [7,8]. Several studies have been carried out on its lithofacies, sedimentary environment, and alkaline lacustrine background, and a model has been proposed for hydrothermal exhalative salt-bearing volcanic–sedimentary deposits in deep lake basins [7,9–13]. Previous research on lamina definitions, types, and combinations [14–20]; their characteristics and formation environment [14,21–26]; and their effect on shale quality [4,27–29] focused on marine and freshwater/brackish-water continental shales. There has been no published work on the role of laminae in alkaline environments. Hence, a study of the mineral compositions, geochemical characteristics, pore types, porosity, diagenetic sequences, and origins of various millimeter-scale laminae will provide insights into lamina development in alkaline lacustrine environments and provide a theoretical reference for lacustrine shale oil exploration and production.

In this study, we quantitatively analyzed the characteristics and distributions of millimeter-scale laminae in the Fengcheng Formation, Mahu Sag, Junggar Basin, and the correlations between them. To fully understand the influence of burial depth on reservoir properties, the samples were taken at specific depth intervals. Equally, in order to avoid the influence of strong heterogeneity and achieve cross-scale characterization of the laminae, a synthetic approach was adopted. The types and combinations of laminae in alkaline lacustrine sediments were qualitatively classified by core scanning at a decimeter level using XRF and by thin-section observation at the centimeter level. Mineral compositions, pores systems, and geochemical indicators were characterized at the millimeter level using rock pyrolysis analysis, Qemscan, nitrogen adsorption, and NMR porosity measurement; at the micron level using scanning electron microscopy and a Modular Automated Processing System; and at the nanolevel using FIB SEM and nano-CT technology.

2. Geological Background

The Mahu Sag is a secondary negative structural unit in the Central Depression in the northwest of the Junggar Basin (Figure 1). The Fengcheng Formation is in the Mahu Sag and is a hybrid sedimentary structure formed by dolomitization, volcanism, and terrigenous clastic sedimentation during a pseudocontemporaneous period in a saline lacustrine environment. It is a significant shale oil layer, rich in laminae [30–32].

The Junggar Basin first evolved as a foreland basin, formed by tectonic activity during the Late Carboniferous–Early Permian [33–35]. The northwestern edge of the basin was extruded by uplifting of the upper mantle, and magma erupted, forming a series of thrust-nappe structures. Due to frequent tectonic movement, there are many fracture zones in the study area, characterized by early formation, long extension, and large break distances. They run through the entire Permian system, accompanied by a series of small secondary faults which are rich in salt minerals. Subduction of the deeper part of the oceanic crust continued until the Middle and Late Permian, when magmatic activity gradually ceased [36]. The Fengcheng Formation in the Mahu Sag has a thickness of 800–1800 m, with a thick west side and thin east side. The main body of the Fengcheng Formation in the Mahu Sag is in the semideep and deep lacustrine facies. There is a large depositional area, and fan-delta deposits are developed in the northern and western margins of the lacustrine basin. From the bottom up, the Fengcheng Formation can be divided into three members (P_1f_1, P_1f_2, P_1f_3), with the P_1f_2 consisting of hybrid sedimentary deposits such as dolomite and argillaceous dolomite with interbedded alkaline minerals [37,38]. The sources of sedimentary material for the P_1f_2 were complex and diverse. Volcanic activity, terrigenous clastic materials, and precipitation of authigenic salt minerals during the salinization process jointly controlled the composition and formation of complex hybrid sediments with low clay contents.

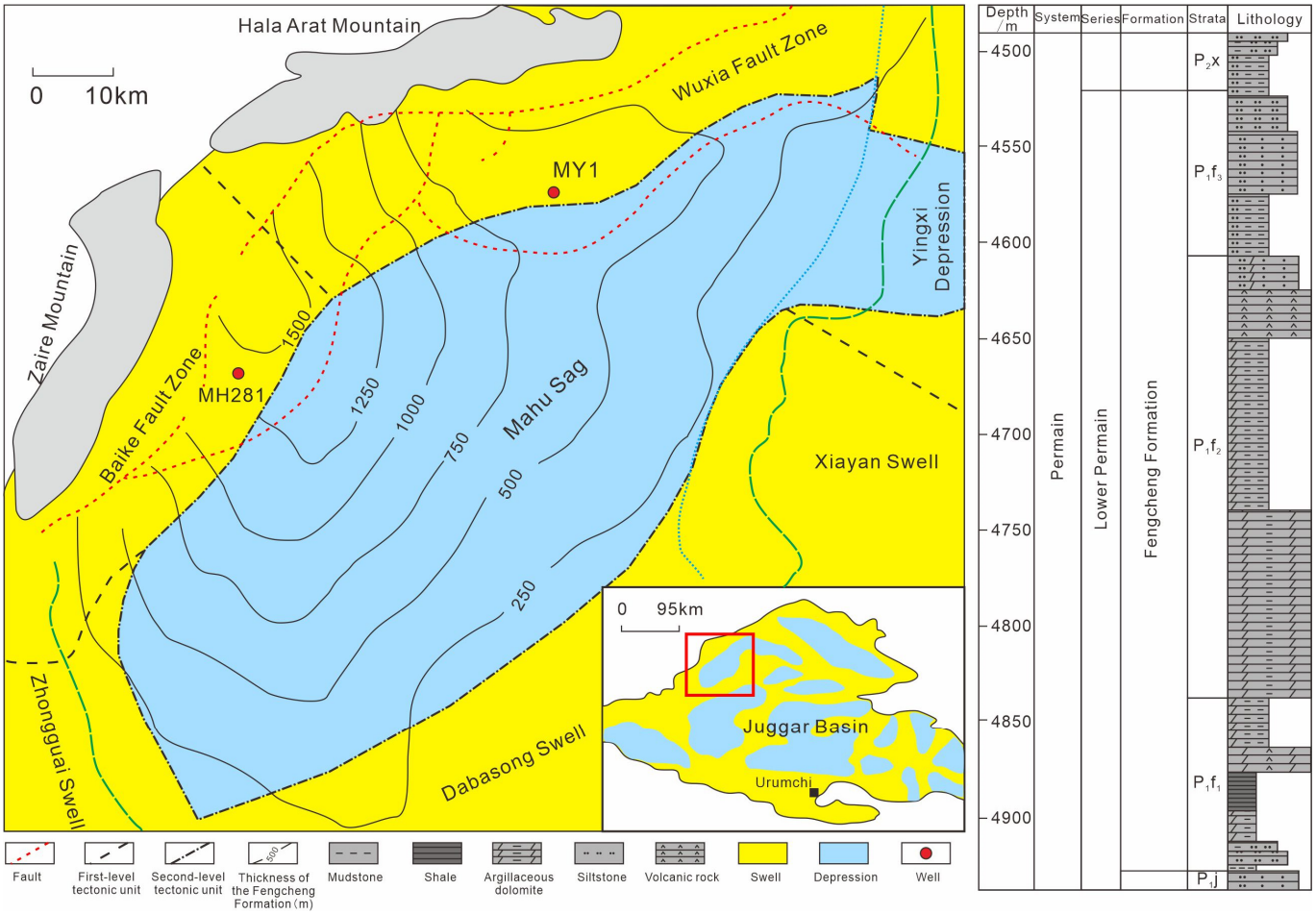

Figure 1. Tectonic background and strata of Mahu Sag in Junggar Basin.

The Mahu Sag is part of the occluded lacustrine formed during the Fengcheng Formation depositional period, which took place in warm, arid, and shallow-water conditions. In the Fengcheng Formation, a type of haloalkaliphilic green algae developed. The algae had the ability to lay a hydrocarbon base that supported the formation of the Mahu Oil Area. The overall strata comprise medium to good source rocks, with mainly type I and II organic matter and a TOC of 0.4~4%, and they are considered to have great shale oil exploration potential [39].

3. Samples and Methods

3.1. Samples

To analyze the characteristics of laminae in the P_1f_2, twenty-two samples were collected from Well Maye 1 and thirty-four samples from Well Mahu 281. Six of the samples were handpicked for further fine study. All the samples were analyzed using X-ray fluorescence spectrometry and slice observation to obtain the element compositions and laminae characteristics of the whole cores. Wire-electrode cutting was used to cut the six samples for fine study into laminae, which produced seventy-one subsamples. These were analyzed for geochemical characteristics, mineralogical composition, and pore structures using TOC content measurement, rock pyrolysis analysis, X-ray diffraction analysis, Qemscan, nitrogen adsorption, NMR porosity measurement, a Modular Automated Processing System, FIB-SEM, and nano-CT technology (Figure 2). The specific experimental procedures were as follows:

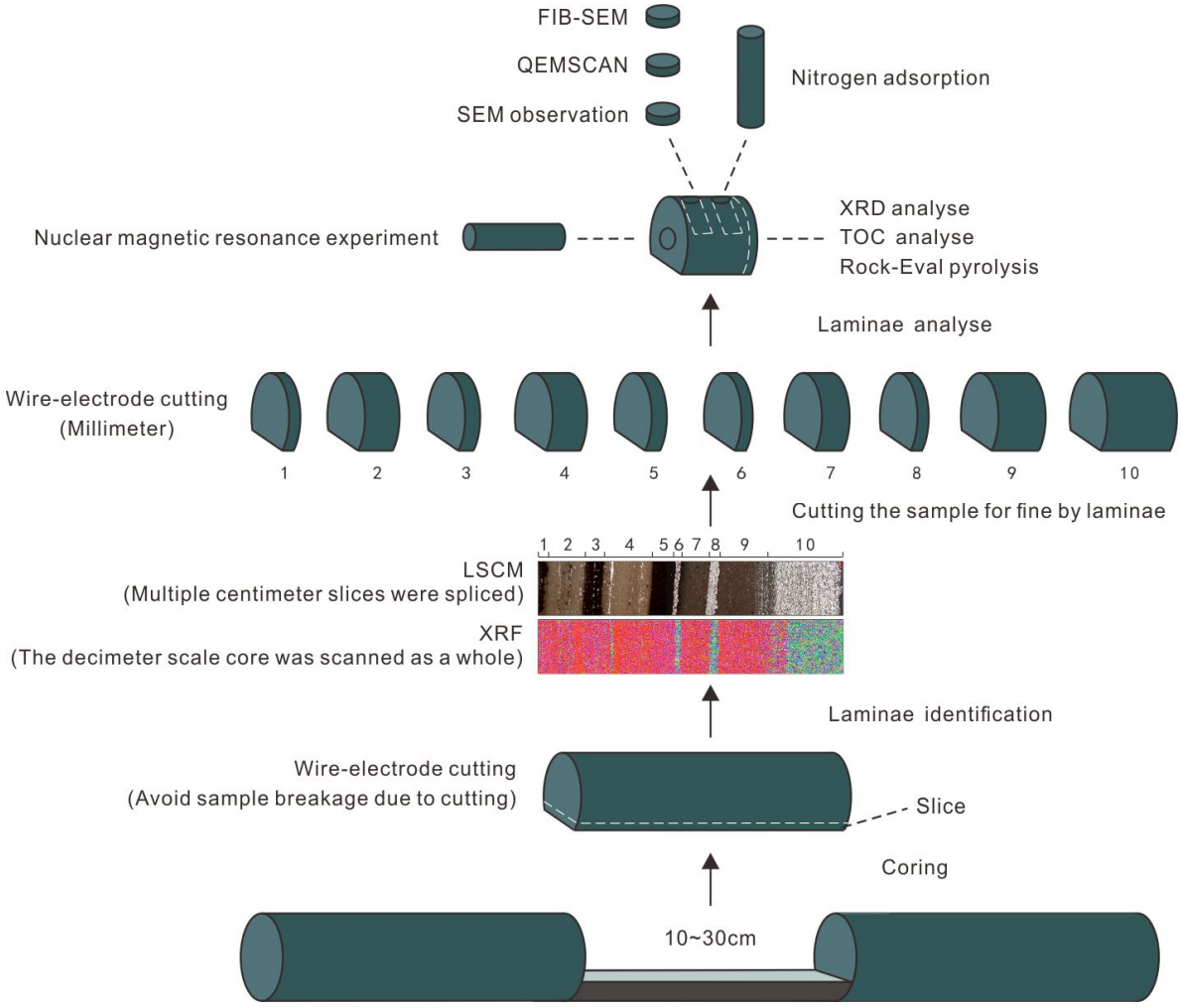

Figure 2. A synthetic analysis method of the P1f2 in Mahu Sag that combines decimeter-scale (XRF scanning of overall cores), centimeter-scale (polarized light microscopy observation), millimeter-scale (XRD, rock pyrolysis analysis, Qemscan, nitrogen adsorption, NMR porosity testing), microscale (scanning electron microscopy), and nanoscale (FIB-SEM and Nano-CT) measurements for laminae evaluation.

3.2. Laminae Division

The laminae and their combinations were identified using core description, slice observation, X-ray fluorescence spectrometry, and mineral composition. Element compositions were determined using tablet–X-ray fluorescence spectrometry (XRF) at the National Energy Tight Oil and Gas Research and Development Center. An M4 TORNADO high-performance microarea X-ray fluorescence spectrometer (detection limit 5×10^{-6}) was used to obtain the qualitative and quantitative characteristics of various elements, which were scanned in 20 μm increments. Elements such as K, Na, Ca, Mg, Al, Si, Fe, and S were extracted for fine identification and characterization of the types and combinations of laminae.

3.3. Geochemical Analyses

Powdered shale samples were analyzed to determine total organic carbon (TOC) percentages by weight using a CS-i carbon and sulfur analyzer (repeatability less than 6%) following China National Standard GB/T19145-2003 (Determination of total organic carbon in sedimentary rock) [40] at the National Energy Tight Oil and Gas Research and Development Center. Other geochemical indicators were obtained using an induction

furnace or Rock-Eval (repeatability less than 5%) following standard GB/T18602-2001 (Rock pyrolysis analysis) [41].

3.4. Mineralogical Composition

Mineral compositions were obtained using XRD and Qemscan for whole-rock minerals and clay minerals at the National Energy Tight Oil and Gas Research and Development Center. A Bruker instrument was used to identify bulk mineralogical compositions and clay minerals, which were scanned at a rate of 0.02°/s between 2.6° and 45° in 2θ at room temperature (20 °C). Petrographic composition can also be determined using QEMSCAN, which performs point-by-point energy spectrum analysis of samples to allow comparison with a standard mineral information database.

3.5. Optical Characteristic Analyses

Slice observation was conducted in the laboratory of the National Energy Tight Oil and Gas Research and Development Center. A LEICA polarizing microscope was used with both plane-polarized and orthogonal light at various magnifications, from 20× to 400×. The samples were prepared into multipurpose slices, polished on both sides, for observation of the compositions, continuity, shapes, and geometric features of the pores and laminae.

3.6. Pore Structure Measurements

Comprehensive analysis included extracting key attributes and identifying pore types, shapes, sizes, and distributions. Correlations between pore characteristics and geochemical parameters were identified.

Powdered samples, which had been degassed at 110 °C for 12 h to remove water, were analyzed at Peking University using a Micromeritecs ASAP2020 specific surface area analyzer to determine specific surface areas (Brunauer-Emmett-Teller (BET)), pore volumes, and equivalent pore distributions (Barret-Joyner-Halenda (BJH)).

Nuclear magnetic resonance, field emission scanning electron microscopy (SEM) examination, Modular Automated Processing System (MAPS) examination, focused-ion-beam scanning electron microscopy (FIB-SEM) examination, and nano-CT three-dimensional reconstruction were conducted at the National Energy Tight Oil and Gas Research and Development Center.

Square samples, which were manually ground to a fine finish and then ion-polished and carbon-plated, were analyzed for pore characteristics with an Apreo FEI high-resolution field emission scanning electron microscope. Using the watershed method, AVIZO image-processing software (Avizo-20201-Windows64-VC12) was used to identify pores, and the "equivalent circle" model was applied to calculate parameters such as pore diameters and thin-section porosity.

Nano-CT was conducted using an Xraida UltraXRM-L200 (Carl Zeiss, Oberkochen, Germany) following oil and gas industry standard SY/T7410.1-2018 (Determination of three-dimensional pore structure of rocks Part 1: CT scanning method) [42].

FIB-SEM examinations were performed using an FEI Helios NanoLab 650 (FEI Company, Hillsboro, OR, USA) with an accelerating voltage of 1 kV to achieve nanoscale denudation of tight reservoir rocks at a resolution of 0.9 nm and to carry out scanning of individual layers. Three-dimensional images at nanometer resolutions were reconstructed to accurately characterize three-dimensional pore–throat systems in shale reservoirs.

4. Results

4.1. Types and Combinations of Laminae

Five types of laminae were distinguished: felsic laminae (FQL), dolomite laminae (DOL), chert laminae (CL), reedmergnerite laminae (RL), and shortite laminae (SL), as follows:

(1) Felsic laminae: These are primarily composed of quartz and feldspar, followed by dolomite and pyrite, and appear brown under plane-polarized light. The laminae are 0.2~3 cm thick and contain small numbers of organic matter fragments (Figure 3a). The laminae are straight or curved, and their thickness varies slightly. The particle size is generally less than 100 μm, but wide variations in particle sizes give the laminae a mottled light and dark appearance under plane-polarized light.

(2) Dolomite laminae: These are primarily composed of subangular and subcircular dolomite crystals and are colorless under plane-polarized light. The matrix is a mixture of feldspar, quartz, pyrite, and clay minerals. The particle sizes of the dolomite are 50~150 μm and of the matrix minerals less than 10 μm (Figure 3b). In the penecontemporaneous stage, the formation of micritic–microcrystalline dolomite was induced by alkaline-lake microorganisms. The micritic–microcrystalline dolomites were formed by primary precipitation, the replacement of aragonite and high-Mg calcite, and other processes. In the shallow burial stage, the continuous growth of micritic–microcrystalline dolomite and replacement of calcite, tuffs, and other substances formed the silt-sized dolomite. And in the middle burial stage, the dolomite, mostly silt- and fine-sized, was created by the replacement of volcanic materials with dolomitization fluid [43]. The dolomites of DOL are predominantly silt- and fine-sized. The laminae are more than 0.15 cm thick, with bed-parallel fluctuations, and their boundaries are clear.

(3) Reedmergnerite laminae: The primary visible component under plane-polarized light is reedmergnerite, and the laminae are thick. The reedmergnerite particles are colorless, wedge- or rhombus-shaped, and distributed in starlike configurations. The lengths of individual crystals are less than 2 mm, and the aspect ratios are about 2:1 (Figure 3c). They appear gray-white to yellow under orthogonal light, showing biaxial crystals with extinction characteristics and some symmetrical sections. XRF analysis shows that Na and Si are comparatively enriched in the reedmergnerite, and Na, K, Al, and Si are enriched in the matrix.

(4) Shortite laminae: The principal visible component under plane-polarized light is shortite, and the laminae are thick. Shortite particles are colorless and occur in long strips or agglomerate shapes that are mostly distributed along the laminae in two size ranges (width either >2 cm or <5 mm) (Figure 3d). They are biaxial negative crystals with extinction characteristics and second-order light emissions are red in color under orthogonal light. XRF analysis shows that Na and Ca are enriched alongside the shortite and Na, K, Al, and Si are enriched in the matrix.

(5) Chert laminae: These are primarily composed of chert and are colorless. The laminae are 0.1~1 cm thick (Figure 3e). Qemscan reveals that the laminae also contain small amounts of feldspar and pyrite but seldom organic matter. The laminae are smoothly curved with varying thicknesses and clear boundaries.

Four types of laminae combinations are found in the P_1f_2: FQL-DOL, FQL-SL, FQL-RL, and DOL-CL.

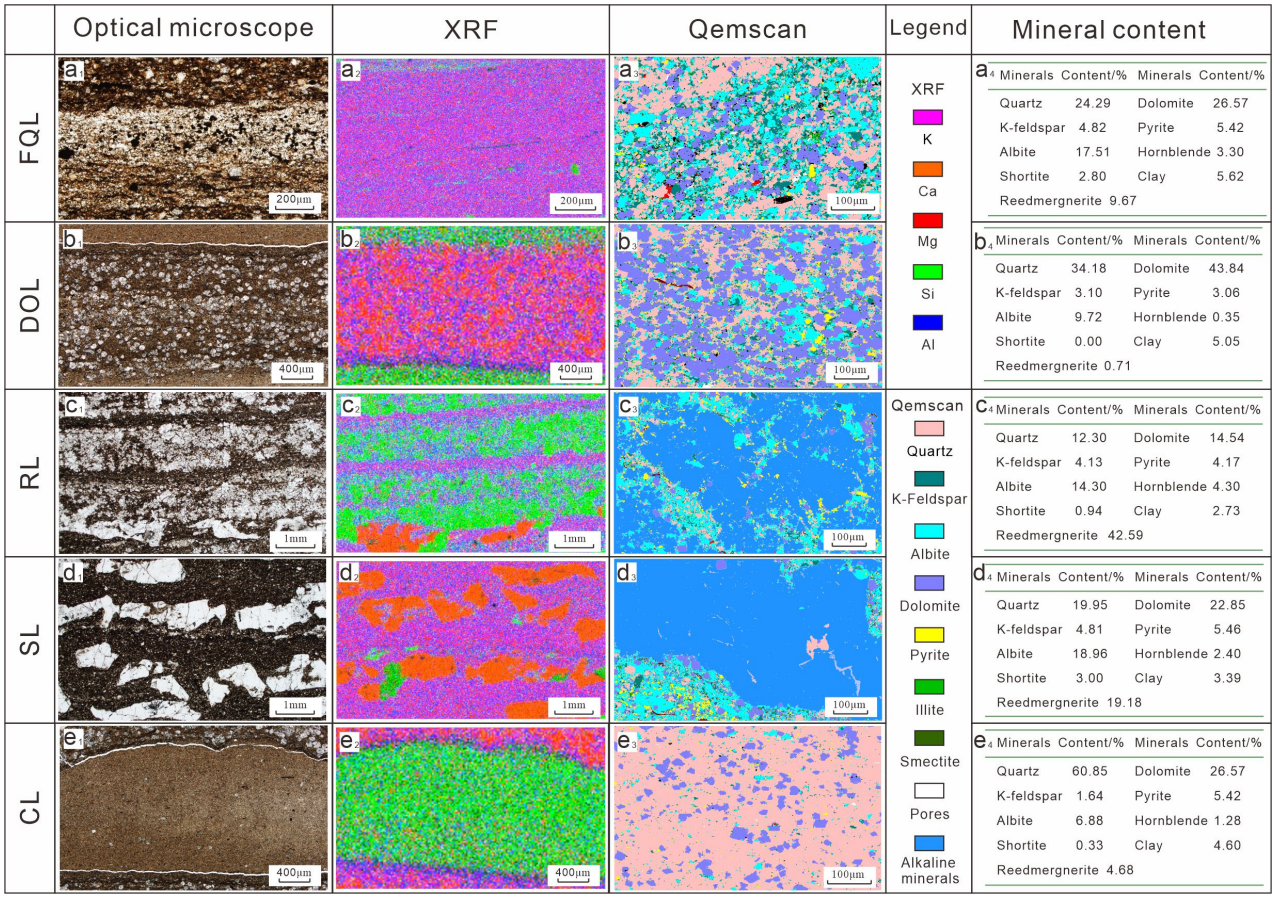

Figure 3. Lamina types and characteristics of the P_1f_2 in the Mahu Sag. (**a$_1$**–**a$_4$**) Felsic laminae, Well Mahu 281, 4943.1 m; (**b$_1$**–**b$_4$**) dolomite laminae, Well Maye 1, 4743 m; (**c$_1$**–**c$_4$**) alkaline mineral laminae, Well Mahu 281, 4865.2 m; (**d$_1$**–**d$_4$**) reedmergnerite lamination, Well Mahu 281, 4664.98 m; (**e$_1$**–**e$_4$**) shortite lamination, Well Mahu 281, 4737.4 m. The images reflect the microscopic characteristics, mineral compositions, and element enrichment of the laminae. The mineral compositions were obtained using XRD.

4.2. Differences between Laminae

The results show that there are distinct differences in depositional environment, mineral compositions, geochemistry, and pore characteristics between different laminae.

4.2.1. Mineral Composition

The fine-grained sediments consist of clastic minerals, alkaline minerals, and organic matter, which form visible boundaries between individual laminae (Figure 4). Clastic minerals include quartz, feldspar, dolomite, pyrite, hornblende, and clay minerals, while the alkaline minerals are predominantly reedmergnerite and shortite. FQL have high contents of felsic minerals and dolomite, including quartz (24.3%), K-feldspar (4.8%), albite (17.5%), and dolomite (26.6%). DOL have dolomite contents of around 43.8%, followed by quartz, and the contents of alkaline minerals are markedly enhanced in RL and SL. CL have dramatically increased chert content (60.9%) but low K-feldspar.

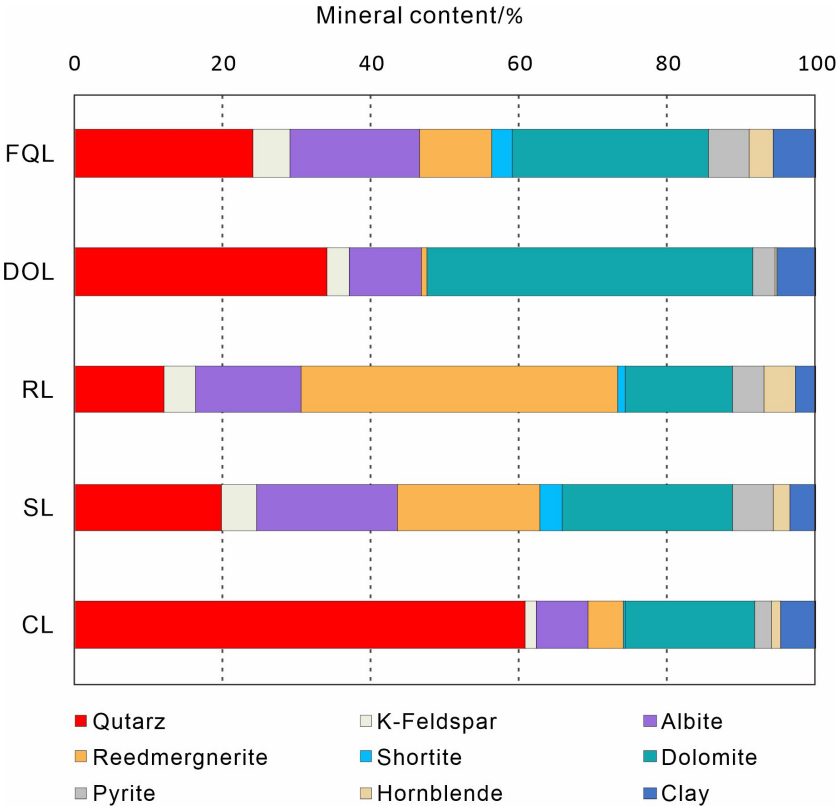

Figure 4. Mineral compositions of laminae by XRD in the P_1f_2 in the Mahu Sag.

4.2.2. Geochemical Characteristics

The TOC contents of samples from different laminae range from 0.2% to 1.7%, concentrated around 0.8% to 1.5% (Figure 5). The average TOC contents of the six lamina types are as follows: FQL, 1.30%; DOL, 0.91%; RL, 1.27%; SL, 1.24%; and CL, 1.00%. The FQL and RL samples have higher TOC values than the others. The RL samples also show high values for production index (PI). However, there is a negative correlation between TOC and oil saturation index (OSI). DOL and CL have higher OSI values than the other types, with average values of 187.9 and 177.21 mg/g TOC, respectively. On the whole, FQL and RL have the best oil-bearing properties.

4.2.3. Pore Characteristics

Organic pores, inorganic pores, and microfractures all occur in the P_1f_2. The inorganic pores are mainly intragranular, intercrystalline, and dissolution pores. The dissolution pores mainly occur in carbonate, quartz, and feldspar. Organic pores are less developed and are mostly found in the organic matter associated with clay minerals and pyrite. They are generally elliptical or stomatic in shape with no specific orientation and are predominantly small in size. Inorganic pores are dispersed among debris particles in nondirectional arrangements with poor pore connectivity. They are triangular, angular, or rectangular in shape. Microfractures mostly occur between mineral grains or between mineral grains and clumps of organic matter and are strip-shaped.

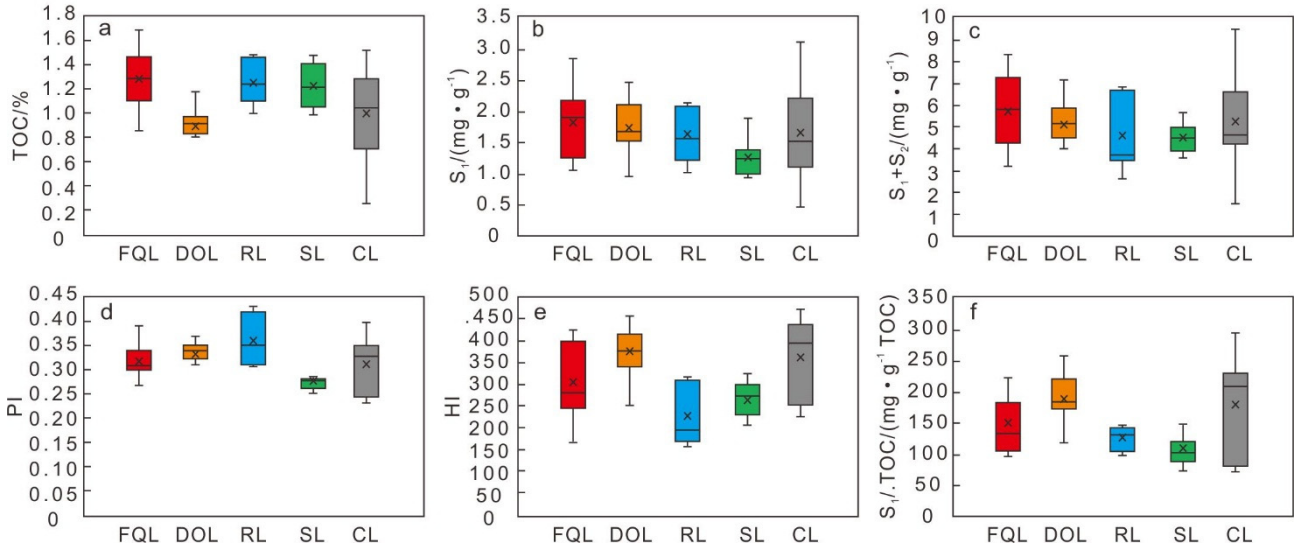

Figure 5. Comparison of organic geochemical characteristics of laminae in the P_1f_2 in the Mahu Sag. (**a**) The TOC value of laminae in the P_1f_2; (**b**) The S_1 value of laminae in the P_1f_2; (**c**) The $S_1 + S_2$ value of laminae in the P_1f_2; (**d**) The PI value of laminae in the P_1f_2; (**e**) The HI value of laminae in the P_1f_2; (**f**) The S_1/TOC value of laminae in the P_1f_2. PI = $S_1/(S_1 + S_2)$; HI = S_2/TOC; OSI = S_1/TOC.

(1) Pore types and characteristics

The adsorption curves of the different laminae are all "S"-shaped and belong to type H_3 in the International Union of Theoretical and Applied Chemistry (IUPAC) classification. When relative pressure (P/Po) is greater than 0.9, adsorption capacity increases rapidly. The desorption curves almost coincide with the adsorption curves, indicating open wedge-shaped or slit-type parallel-plate pores.

The pores in FQL are mostly scattered intergranular pores of large size, densely packed dissolution pores of uniformly small size, and organic pores (Figure 6a–d). DOL contain mostly dissolution and intercrystalline pores (Figure 6e–h). The dissolution pores are primarily found in dolomite and in feldspar, which is on the edges of dolomite crystals. Feldspar dissolution pores are much more common than dolomite dissolution pores. The imporous particles are mostly alkaline minerals. RL contain intercrystalline pores, dissolution pores, and highly developed organic pores, as well as small numbers of intragranular pores (<2%) (Figure 6i–l). SL are mainly composed of intercrystalline pores, dissolution pores, and microfractures. The microfractures mostly occur in shortite in proportions less than 5% and with aspect ratios greater than 10 (Figure 6m–p). CL contain mostly dissolution pores in chert (Figure 6q–t).

(2) Pore size distribution

Nanopores predominate in the fine-grained sediments of the P_1f_2. In this study, various methods were used to measure pore size distributions. NMR analysis shows that the pore size distributions of all lamina types are bimodal (Figure 7a–c). The BJH desorption cumulative pore volumes are highest when the average pore width is less than 2 nm, followed by those of pores in the range 7~15 nm. MAPS data show that the pore sizes of all laminae vary in the range of 20~100 nm. Generally, pore sizes in the P_1f_2 are mainly less than 100 nm. The proportions of large pores are higher in FQL, DOL, and RL than in SL and CL.

(3) Porosity

Various methods were used to measure the porosities of individual laminae. Using NMR, the average porosities were as follows: FQL, 2.06%; DOL, 1.21%; RL, 2.63%; SL, 1.28%; and CL, 1.08% (Figure 7d). According to the nitrogen adsorption results, the average porosities were as follows: FQL, 3.00%; DOL, 1.88%; RL, 2.51%; SL, 2.64%; and CL, 2.02%

(Figure 7e). Overall, FQL have the best porosity, followed by RL. SL have medium porosity, and DOL and CL show the poorest porosity.

(4) Plane porosity

A total area of 625 μm × 625 μm (625 small areas of 25 μm × 25 μm) in the SEM image was used to count the pores in individual laminae. The average plane porosities are as follows: FQL, 52.9%; DOL, 58.7%; RL, 60.6%; SL, 53.4%; and CL, 26.6% (Figure 7f). Although intragranular pores rarely occur in the reedmergnerite crystals in RL, pores in matrix minerals—composed of felsic, dolomite, and clay minerals—are extremely common and contribute significantly to plane porosity (Figure 8).

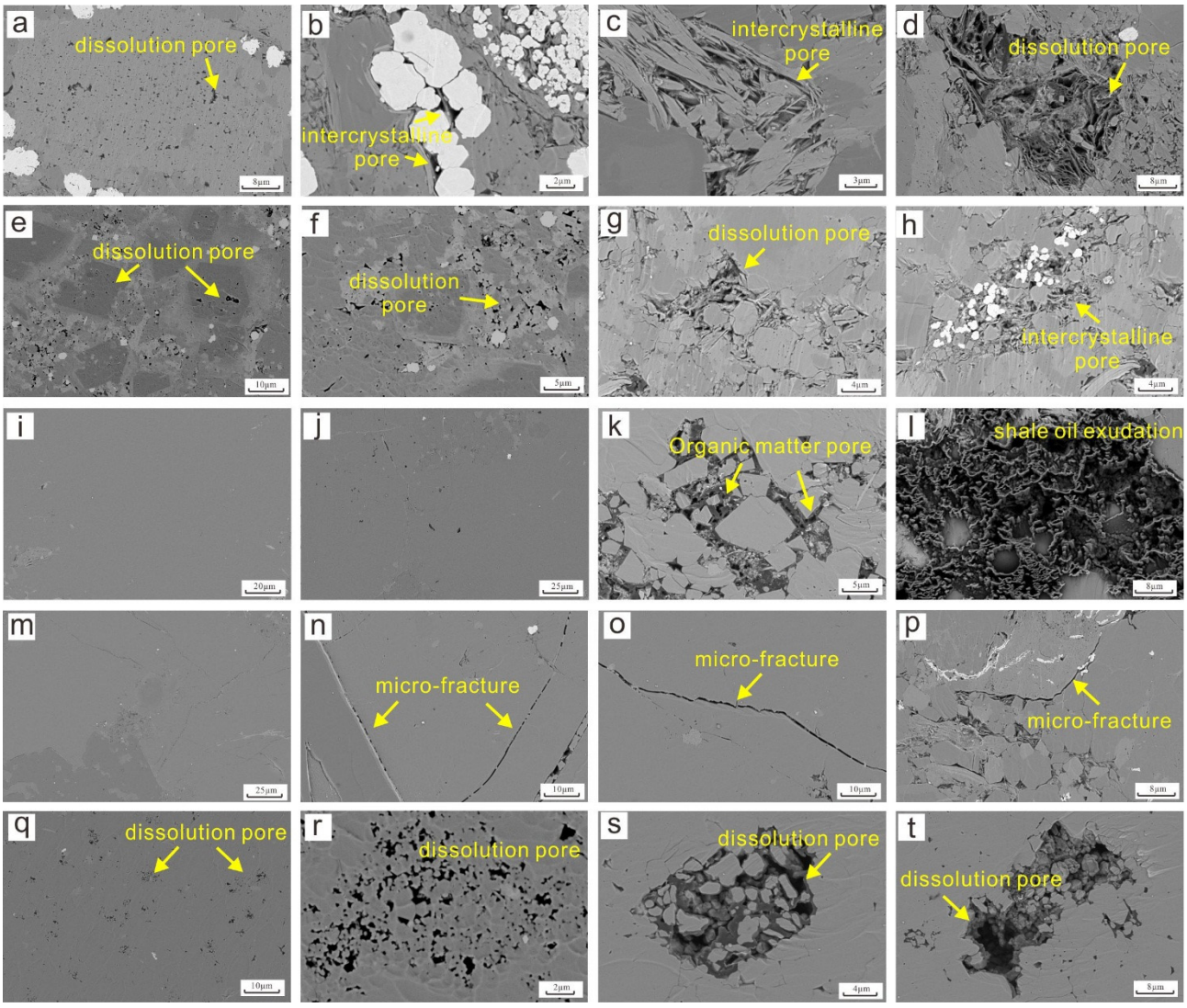

Figure 6. Pore characteristics of individual laminae under SEM, showing pore types, shapes, size, and distribution. (**a**) Feldspar dissolution pores in FQL; (**b**) pyrite intercrystalline pores in FQL; (**c**) clay intercrystalline pores and organic matter dissolution pores in FQL; (**d**) organic matter dissolution pores in FQL; (**e**,**f**) dolomite dissolved pores and feldspar dissolved pores in DOL; (**g**,**h**) intercrystalline pores in DOL; (**i**) sodalite crystals in RL; (**j**) intercrystalline pores and organic matter dissolution pores in RL; (**k**) organic matter dissolution pores in RL; (**l**) crude oil exudation in RL; (**m**) solite crystals in SL; (**n**–**p**) microfractures in SL; (**q**–**t**) dissolution pores in CL.

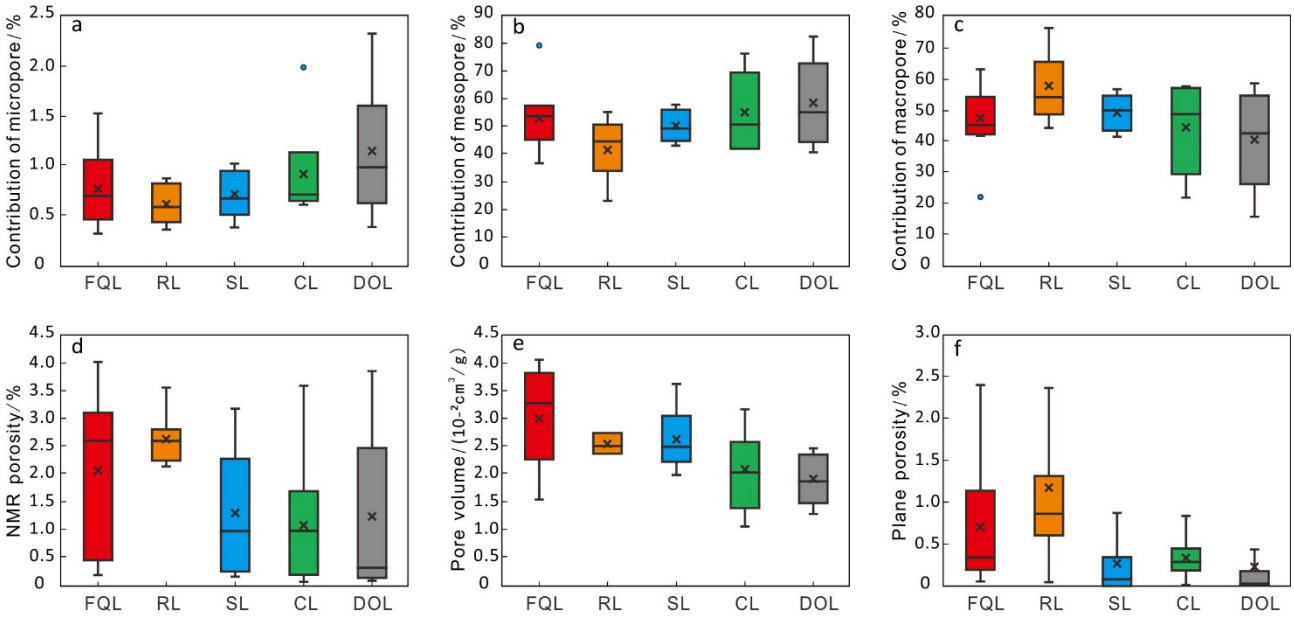

Figure 7. Pore parameters of the P_1f_2 in the Mahu Sag. (**a**) T2 spectrum; (**b**) average width of pores from BET; (**c**) equivalent diameter distribution of pores from MAPS; (**d**) porosity from NMR; (**e**) porosity from BET; (**f**) porosity from MAPS.

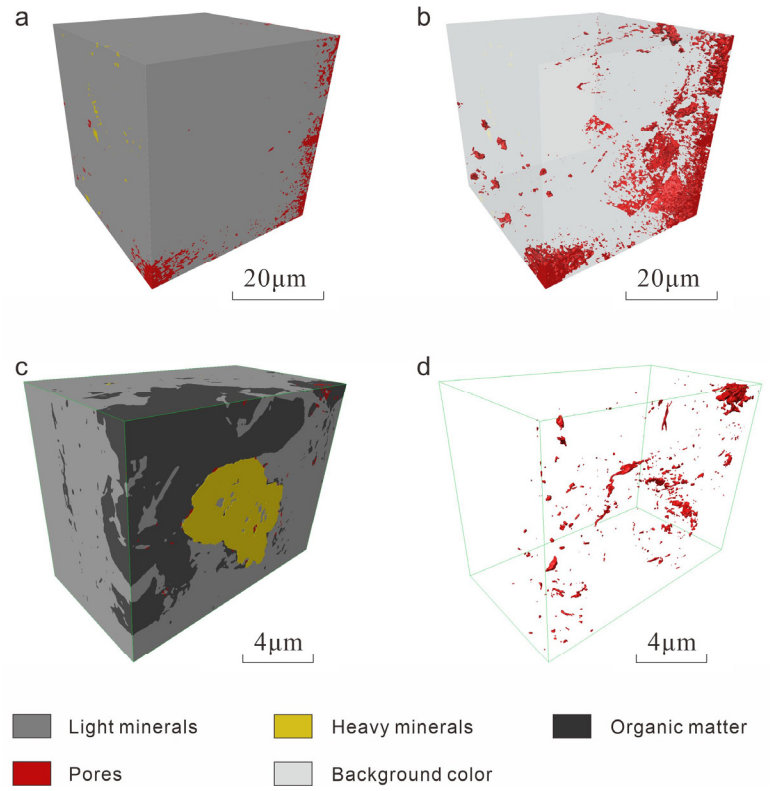

Figure 8. Nano-CT pore characteristics. (**a**) RL in nano-CT; (**b**) pore development of RL in nano-CT; (**c**) RL in FIB; (**d**) pore development of RL in FIB.

4.2.4. Lamina Density

The figures show an obvious positive correlation between porosity and TOC content (Figure 9a). The acids that dissolve minerals mostly come from organic matter, and the intensity of dissolution is controlled by the content of organic matter, the concentration of organic acid, the mode of occurrence of the soluble minerals and organic matter, etc. There

is, however, a negative correlation between lamina density and TOC content (Figure 9b). The development of laminae reflects periodic fluctuations in sedimentation rates and hydrodynamic conditions, indicating an unstable water environment. Strong laminae indicate frequent variations in hydrodynamic conditions during deposition, which is not conducive to the preservation of organic matter and therefore affects organic carbon content and pore characteristics.

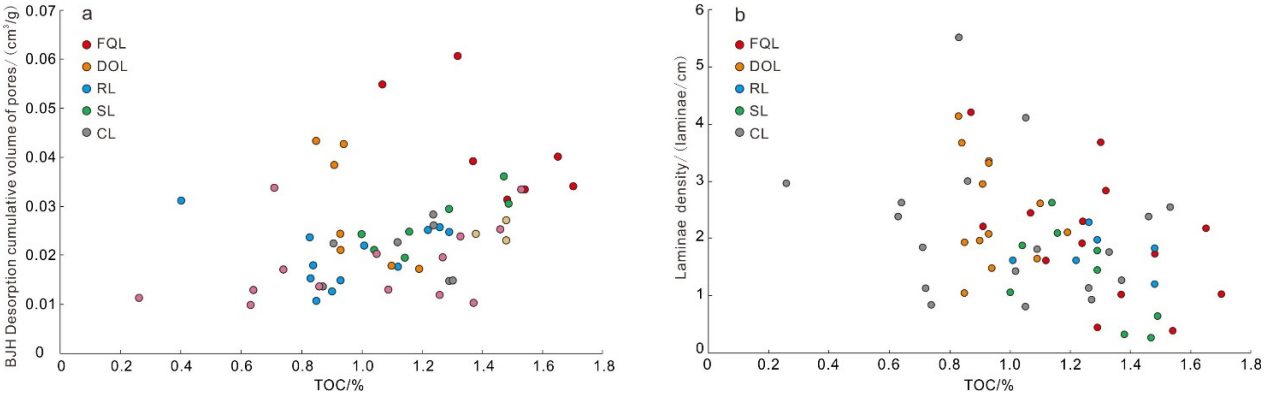

Figure 9. Relationship between total organic carbon and porosity and laminae density. (**a**) Relationship between total organic carbon and BJH desorption cumulative volume of pores; (**b**) relationship between total organic carbon and laminae density.

4.2.5. Correlation Analysis

The average values of the parameters that characterize reservoir properties (pore volume—V, specific surface area—S) and oil content (free hydrocarbon—S1, oil saturation index—OSI, TOC) were used to investigate the relationship between reservoir characteristics and the oil-bearing properties of individual laminae (Figure 10). Overall, FQL and RL show distinctly superior properties. DOL and CL have good oil-bearing properties but the worst pore characteristics. SL do not have any particular advantage over the other types.

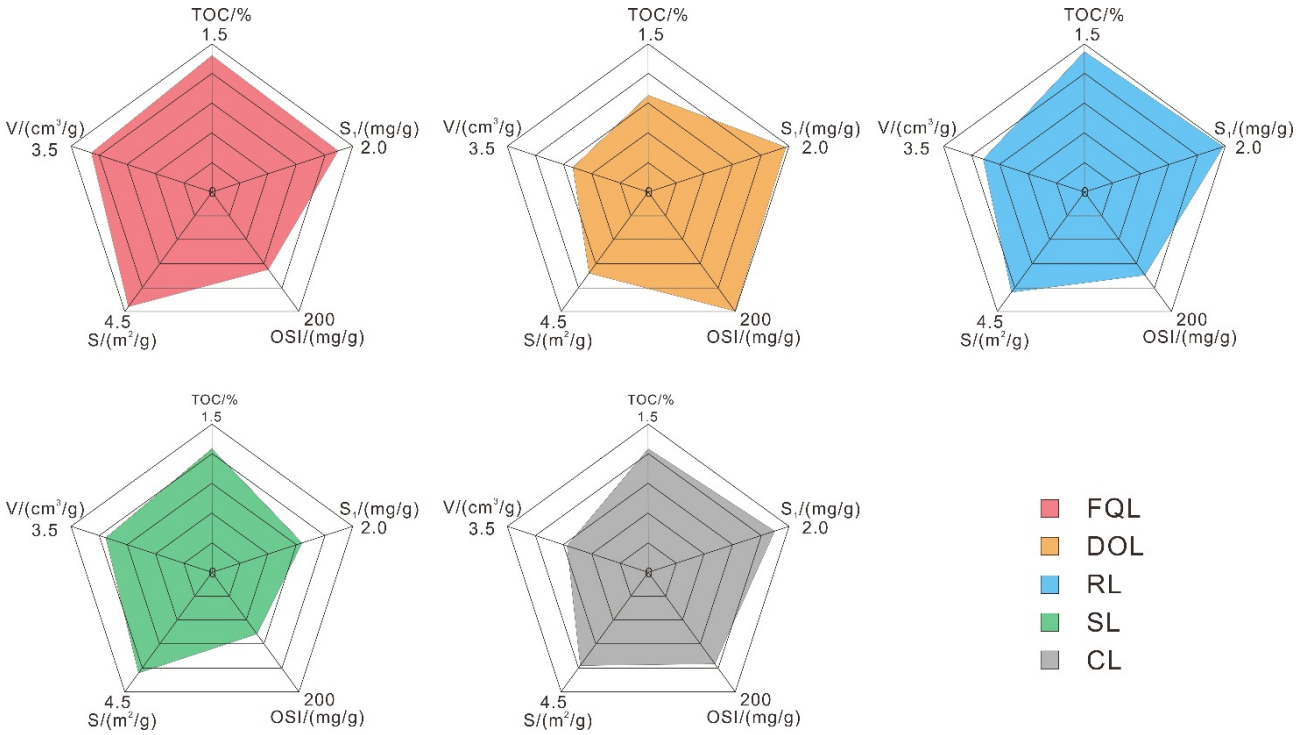

Figure 10. Correlation analysis of reservoir and oil-bearing properties of individual laminae.

4.3. Stratigraphic Organization

Analysis of element abundance and ratios shows a good correlation between paleoclimate and paleowater depth [44] (Figure 11). Generally, the higher the Mg/Ca and Mg/Sr values, the drier and hotter the climate [45]. Mg/Ca values may be low or even extremely low in alkaline layers. During the early stage of the P_1f_2, the Mg/Ca and Mg/Sr values followed a variation pattern of low → high → low [38,44,46]. Combining this with lithology changes suggests that the alkaline minerals present in the middle and late stages of the P_1f_2 could have caused low Mg/Ca and Mg/Sr values even in arid environments. And the climate index C ($C = \sum(Fe + Mn + Ni + Cr + Co + V)/\sum(Ca + Mg + K + Sr + Ba)$) can be used to calculate the paleoclimate; it suggests a semiarid to semihumid condition when C varies from 0.4 to 0.6, and it indicates a semiarid condition when C is 0.2~0.4, and if C is less than 0.2, that indicates an arid condition [38]. The corresponding paleoclimate pattern is therefore humid → semiarid → arid→semiarid. Higher ratios of Mn/Fe and Rb/K indicate shallower water [38]. These ratios show a variation trend of high → medium-low → low → high, and the corresponding pattern for paleowater depths is deep → shallow → shallow → deep [44]. V/(V + Ni) is 0.6~0.84 in a reducing condition and less than 0.6 in an oxygen-enriched environment [38]. The changes in paleowater depth and redox conditions are almost identical to those of the paleoclimate.

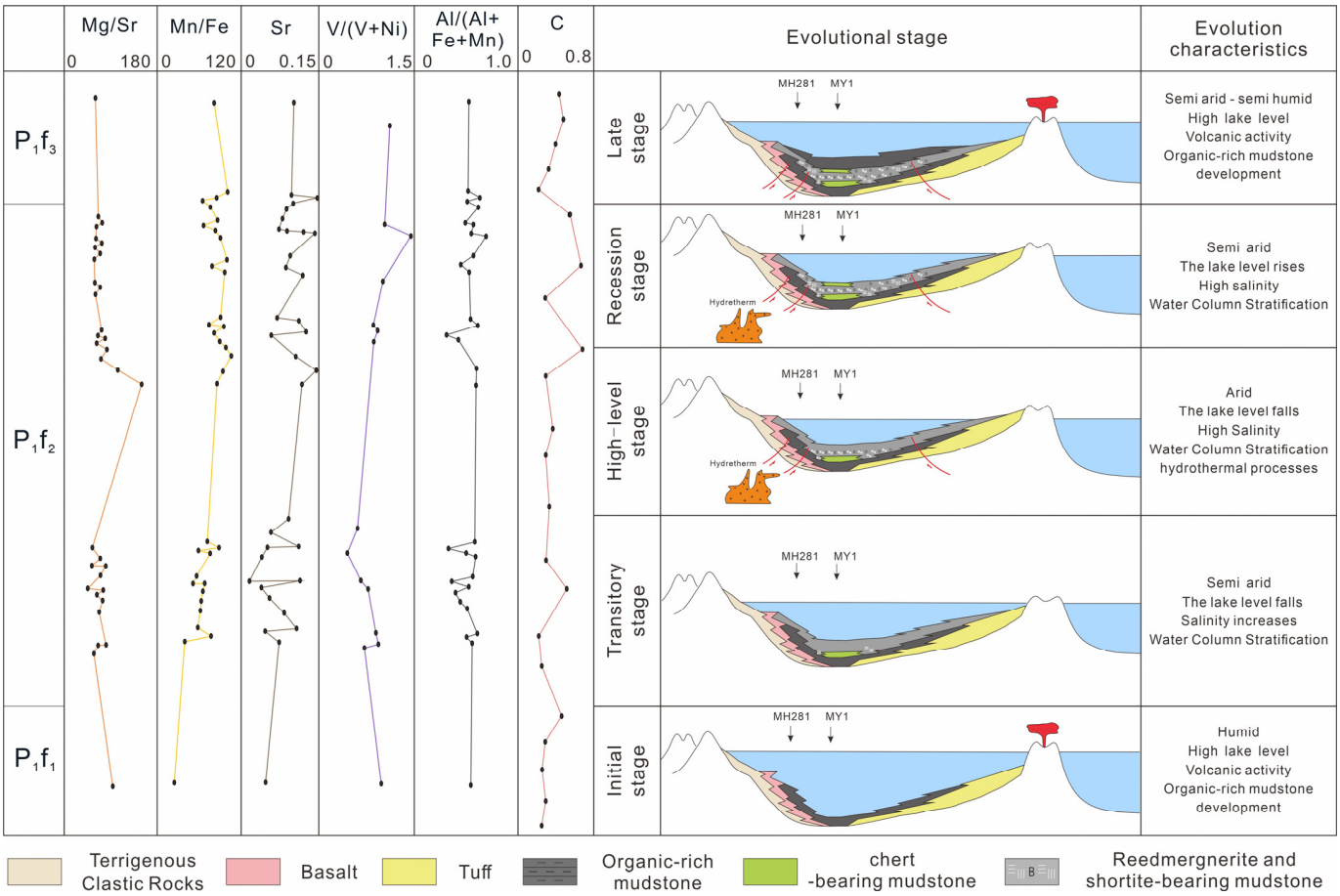

Figure 11. The evolution roughly includes five main stages, which show different sediments under sedimentary condition. It shows a paleowater depth variation trend of deep → shallow → deep and the corresponding paleoclimate variation trend of humid → arid → semiarid, with a salinity of slightly salty → highly salty → slightly salty. Longitudinal variation of paleoenvironmental geochemical parameters of the P_1f_2 in the Mahu Sag is modified from [38,44].

Seasonal wet and dry environment fluctuation appeared during the deposition of the alkaline Fengcheng Formation in the Junggar Basin, with a high degree of salinization and strong evaporation accompanied by frequent volcanic activity and hydrothermal activity which favored the formation of alkaline minerals. Influenced by the changing salinity and environments of the ancient lake in the Mahu Sag, the P_1f_2 can be divided into Mg-Ca carbonate minerals, Mg-Ca-Na carbonate minerals, and Na carbonate minerals according to the types of cations [47]. With increasing salinity, the mineral composition shows a change from Mg-Ca carbonate minerals (dolomite-dominated) to Mg-Ca-Na carbonate minerals (shortite-dominated) and Na carbonate minerals (reedmergnerite-dominated) (Figure 12).

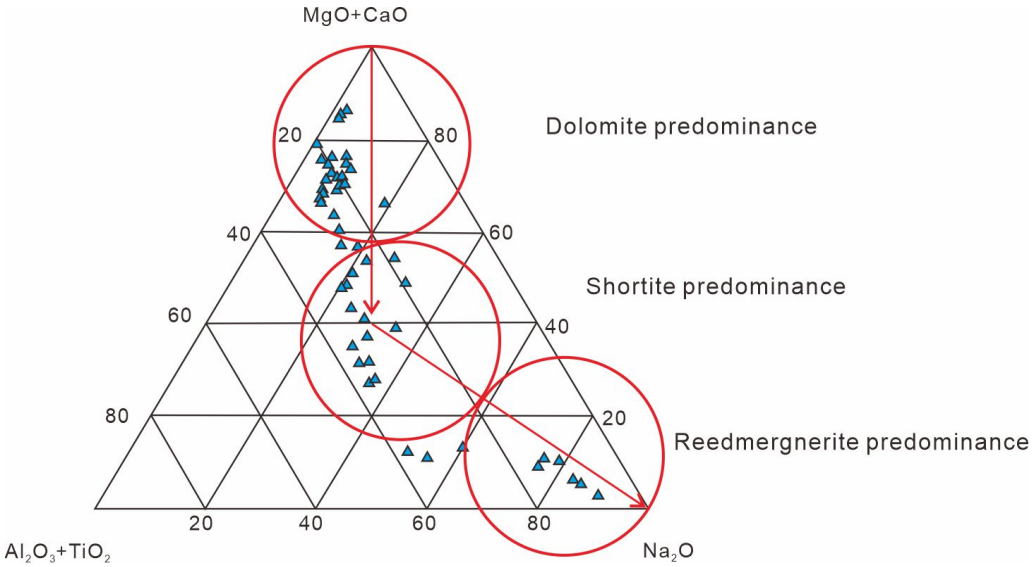

Figure 12. The diagenetic evolution sequence of the P_1f_2 in the Mahu Sag.

Influenced by material sources, the Fengcheng Formation developed a large amount of terrestrial-source clastic sedimentary with a high degree of felsic laminae. As a result of the event deposition, a large number of gravity deformation structures (load structures and sand ball–sand pillow structures), hydroplastic deformation structures (water escape structures and salt dike structures), and brittle deformation structures (intralayer faulting, step faults, and microfractures) are visible in the Fengcheng Formation (Figure 13).

The shale in the continental lacustrine basin has a wealth of material sources, and the materials created in the shale laminae comprise endogenous, volcanic–hydrothermal, and terrestrial components. Among these, endogenous materials are nonexotic materials like carbonate minerals and calcareous microbial crusts formed by evaporation and microbial activities in the basin [48,49]. Special alkaline minerals fall into this genetic mechanism. Volcanic–hydrothermal materials are sediments formed by volcanic tuff and volcanic glass, brought into the basin through precipitation through volcanism and deep hydrothermal action, which is the cause of chert. Terrestrial-source materials are those formed by the transportation of quartz, feldspar, and clay minerals, etc., along the direction of the source supply [50].

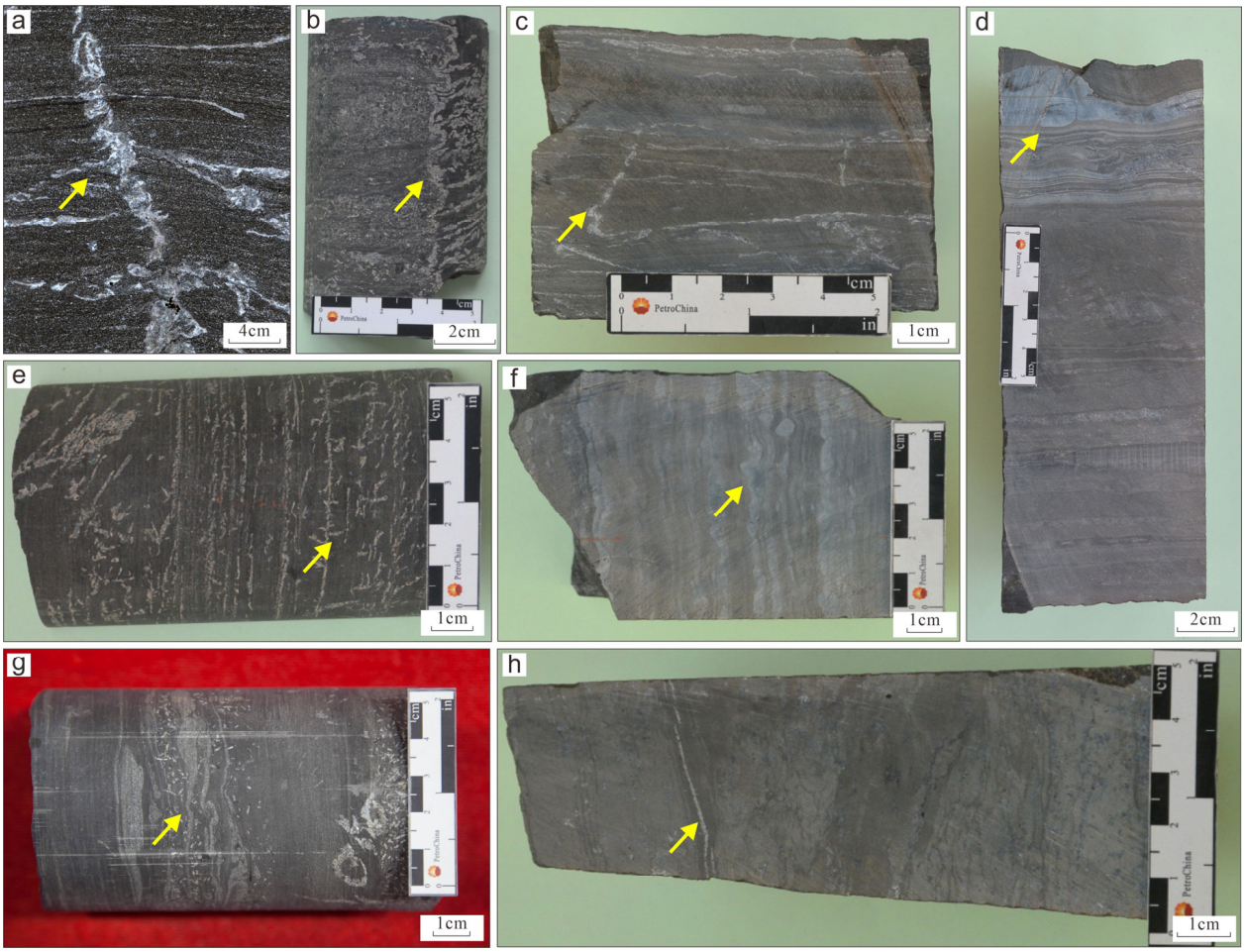

Figure 13. The deformation structures of shale in Fengcheng Formation. (**a**) Water escape structures; (**b**) salt dike structures; (**c**) microfractures; (**d**) hydroplastic deformation structures; (**e**) water escape structures; (**f**) sand ball–sand pillow structures; (**g**) soft sediment sliding structure; (**h**) microfracture.

5. Discussion

5.1. Laminae Sedimentary Mechanism

Single and mixed sources make up the material sources of the alkaline lacustrine shale series in the Junggar Basin, and this study reveals that the shale was generated by three different depositional methods: terrestrial-source still water deposition (TSSWD), intrasource deposition (ISD), and hybrid-source still water deposition (HSSWD).

FQL are dominated by terrestrial input of felsic minerals and clay, with a low content of organic matter and endogenous sedimentary minerals, and are from single-terrestrial-source still water deposition (Figure 3a). DOL are mainly composed of terrestrial inputs (felsic minerals, clay) and endogenous dolomite and are from hybrid-source still water deposition, with no dolomite of a single endogenous sedimentary origin (Figure 3b). RL and SL are mainly composed of a combination of terrestrial inputs (feldspathic minerals, clay minerals) and endogenous alkaline minerals (reedmergnerite and shortite), which are from hybrid-source still water deposition (Figure 3c,d). CL are mainly endogenous chert, which is from single intrasource deposition (Figure 3e). Vertically, there are several interstratified deposits of terrestrial FQL and mixed DOL, mixed DOL and endogenous CL, and terrestrial FQL and mixed RL/SL.

The FQL-DOL combination, which developed in terrestrial-source still water deposition and hybrid-source still water deposition, features high feldspar, quartz, and carbonate mineral composition. The excellent reservoir space, moderate fracture development, and oil traces visible in the core all point to favorable reservoir characteristics in the FQL-DOL

combination. High levels of gray-white spots or long stripes of alkaline mineral development can be detected in the FQL-RL combination and FQL-SL combination core sample, which is light gray. It shows well the fracture development and medium pore development. And it developed in terrestrial-source still water deposition and hybrid-source still water deposition. The DOL-CL combination shows limited pore space. And the core is light gray with gray-black siliceous strips which are high in chert mineral. The DOL-CL combination developed in intrasource deposition and hybrid-source still water deposition.

5.2. Sedimentary Evolution

Deposition of the P_1f_2 took place in a high-salinity reducing environment and was accompanied by at least two invasions of hydrothermal fluids (Figure 11). The paleoclimate was relatively humid → semiarid → arid → semiarid, with the paleowater depth and paleosalinity changing accordingly [44]. We distinguished the sedimentary evolution of the P_1f_2 into five stages in accordance with Zhang's five stages of paleoenvironmental evolution [44] (Figure 14). And combined with thin sections, laminae distribution was systematically studied (Figure 15). Affected by volcanic activity, hydrothermal injections, and paleoclimate, the distribution of alkaline minerals is limited.

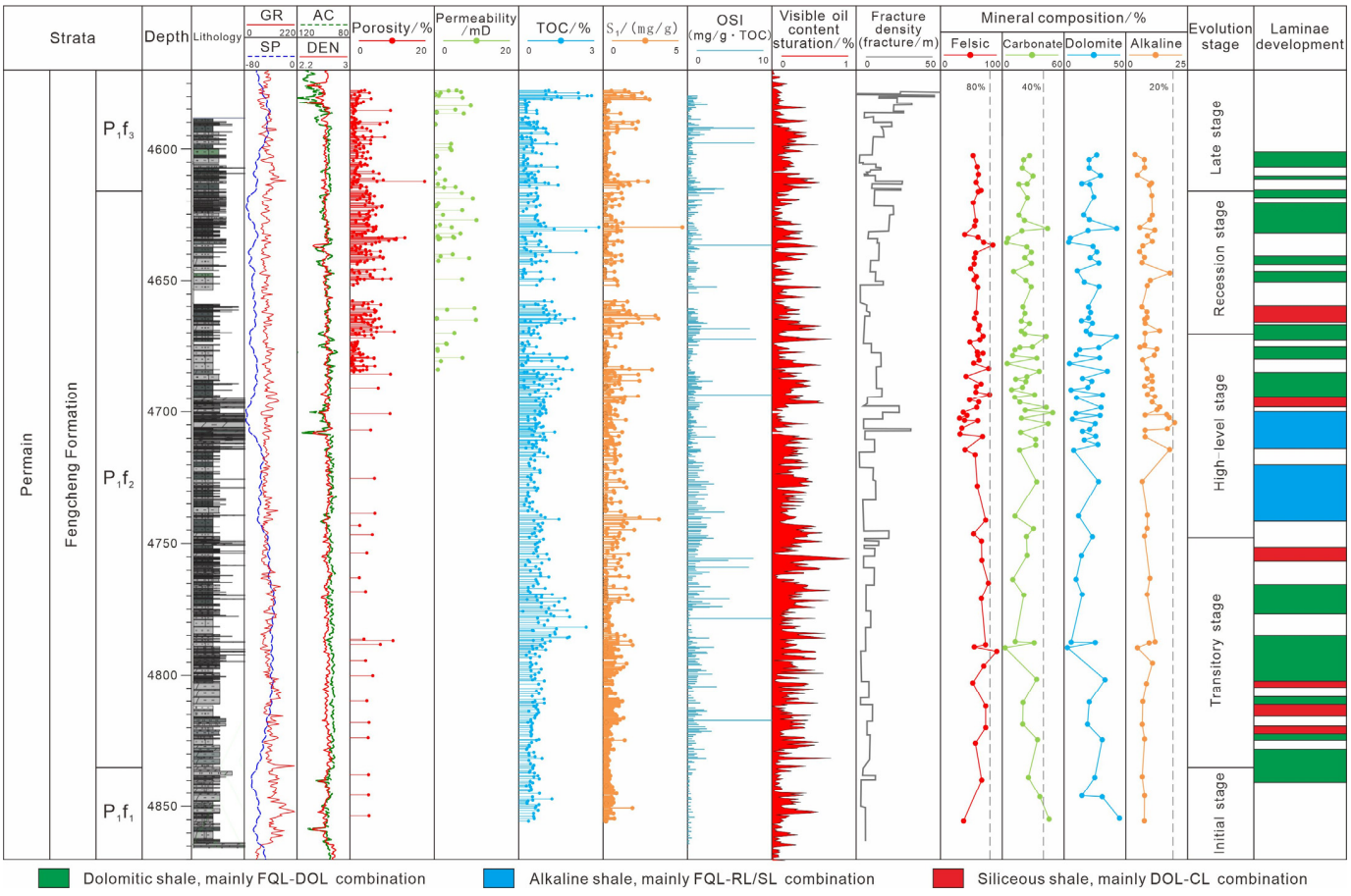

Figure 14. Laminae combinations and origin of the Well MY1 in the Mahu Sag. Comprehensive diagram showing laminae combinations, diagenetic sequence, and sedimentary condition evolution. Laminae combination variation roughly includes three main stages, which are mainly caused by pH, chemical weathering of granitic and rhyolite rock, biological metabolism, volcanic activity, and hydrothermal fluid.

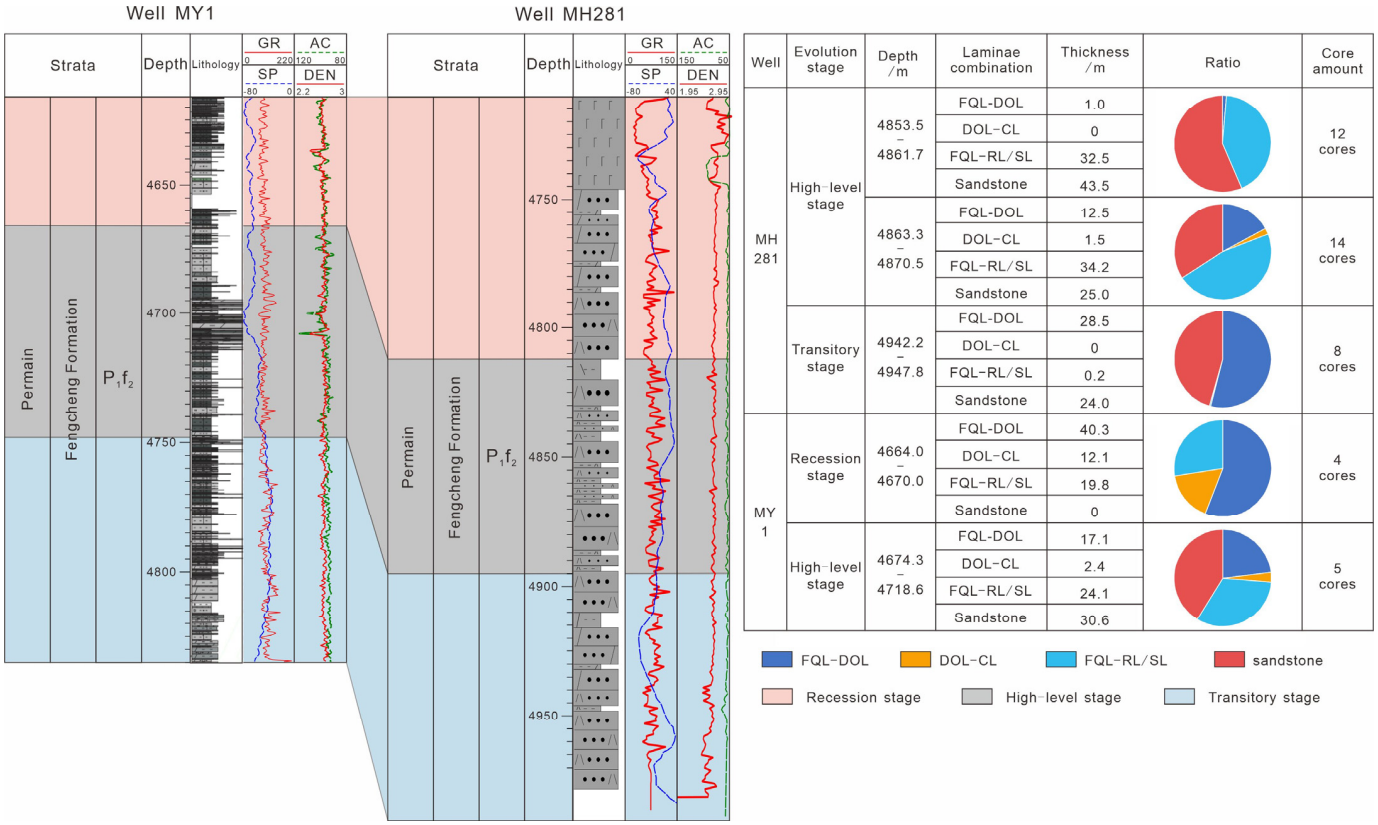

Well	Evolution stage	Depth /m	Laminae combination	Thickness /m	Ratio	Core amount
MH 281	High-level stage	4853.5 – 4861.7	FQL-DOL	1.0		12 cores
			DOL-CL	0		
			FQL-RL/SL	32.5		
			Sandstone	43.5		
		4863.3 – 4870.5	FQL-DOL	12.5		14 cores
			DOL-CL	1.5		
			FQL-RL/SL	34.2		
			Sandstone	25.0		
	Transitory stage	4942.2 – 4947.8	FQL-DOL	28.5		8 cores
			DOL-CL	0		
			FQL-RL/SL	0.2		
			Sandstone	24.0		
MY 1	Recession stage	4664.0 – 4670.0	FQL-DOL	40.3		4 cores
			DOL-CL	12.1		
			FQL-RL/SL	19.8		
			Sandstone	0		
	High-level stage	4674.3 – 4718.6	FQL-DOL	17.1		5 cores
			DOL-CL	2.4		
			FQL-RL/SL	24.1		
			Sandstone	30.6		

Figure 15. Laminae development of Well MH281and Well MY1.

The early and middle stages of the P_1f_2 correspond to the statistical stratigraphy of the Well MH281, while the middle and late stages of the P_1f_2 correspond to the statistical stratigraphy of the Well MY1 (Figure 15). According to the statistics, FQL-DOL combinations and sandstone deposits predominated in the early stages of the Well MH281. Afterwards, FQL-RL/SL combinations gradually took over the leading position, with additional contributions from FQL-DOL combinations and sandstone deposits. The FQL-RL/SL combinations then displayed a declining trend and progressively moved into the late stage. In the Well MY1, DOL-CL combinations, FQL-DOL combinations, and sandstone deposits were mostly deposited between 4721.4 m and 4726.8 m. Subsequently, a substantial amount of FQL-RL/SL combinations was formed, considerably reducing the amount of DOL-CL combinations and FQL-DOL combinations. At 4664.0 m~4670.0 m, the fraction of DOL-CL combinations and FQL-DOL combinations grew dramatically, with DOL-CL combinations dominating, while the proportion of DOL-CL combinations showed a declining trend.

The evolution occurred as follows:

1. The initial stage of salinization occurred during the late P_1f_1 and the early P_1f_2 under semideep lacustrine conditions. The climate was humid and the lake level high, with strong injection of water and weak evaporation [44]. Volcanic activity provided rich nutrients for aquatic organisms, resulting in high organic matter abundance. These reducing conditions were conducive to the accumulation and preservation of organic-rich mudstone. Salinity at this stage was still low and had not yet reached saturation. When the primary stage of salt mineral precipitation began, Ca^{2+} and Mg^{2+} combined with CO_3^{2-} [47] before Na^+ and precipitated to form Mg and Ca carbonate minerals that interbedded extensively with the mudstones. In this period, the FQL-DOL combination was well developed, with little development of alkaline minerals (Figure 16).

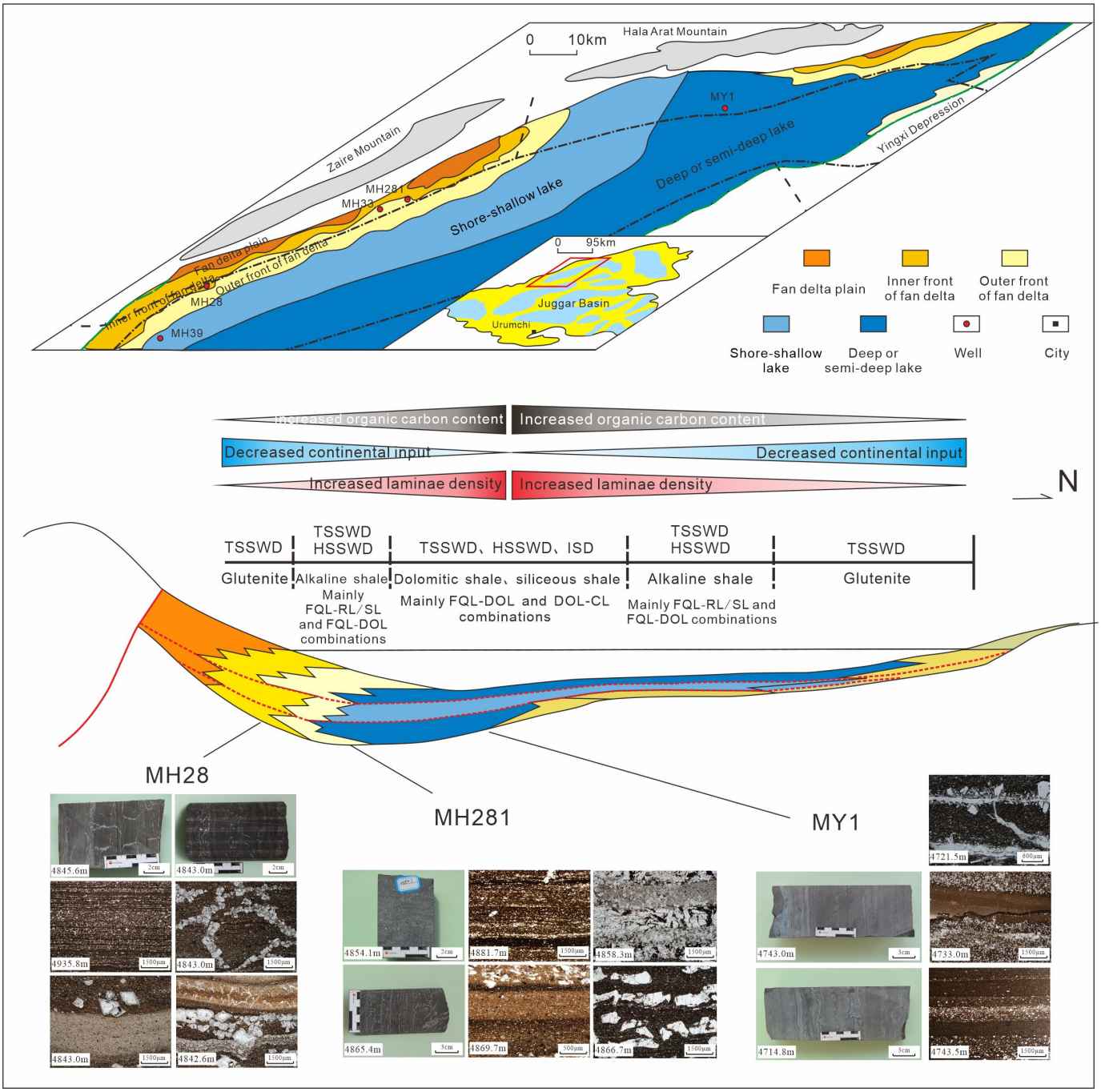

Figure 16. Laminae distribution of the P_1f_2 in the Mahu Sag. TSSWD: terrestrial-source still water deposition; ISD: intrasource deposition; HSSWD: hybrid-source still water deposition.

2. The transitional stage of salinization occurred during the early–middle P_1f_2 deposition under shallow and relatively dry semideep lacustrine conditions. The intensity of water injection was less than evaporation, resulting in falling lake levels. The supply of terrigenous debris was inadequate. With the increasing salinity, the sediments gradually alkalized, accompanied by water stratification. Volcanic activity and microbial consumption also gradually alkalized the water, encouraging Na^+ to participate in crystallization to form shortite [12,47]. At the edges of the basin, the most common alkaline mineral was shortite, in low–medium concentrations and with large crystal sizes, indicating the rapid deposition. In this period, the FQL-DOL combination, FQL-SL combination, and DOL-CL combination were well developed. FQL-DOL and

FQL-SL combinations formed at the edges of the basin. Towards the center of the basin, the chert bands developed, forming the DOL-CL combination (Figure 16).

3. The high-level stage of salinization occurred during the middle P_1f_2 under arid conditions in a shallow lacustrine environment. In this stage, the pH > 9, and hydrothermal fluids and strong microbial activity contributed significantly to salinization and alkalization [12]. As salinity increased, water stratification became more pronounced [51]. With the influx of hydrothermal fluids, evaporative salt minerals developed in large quantities, ushering in a period of great richness of alkaline-bearing sedimentary layers. In an arid climate, the water was further concentrated and salinized, and large amounts of boron combined with hydrothermal fluids to form reedmergnerite [12,47]. When pH values exceed 9, the solubility of silica increases exponentially, so silicate contents dropped dramatically. The FQL-SL/RL combination principally developed during this stage. And the FQL-DOL combination continued to develop during this period in a relatively small percentage.
4. The recession stage of salinization occurred during the middle–late P_1f_2 deposition, under semiarid to arid conditions with slightly rising lake levels and decreasing salinity in a shallow lacustrine environment, and the pH < 9 [12,44]. The influx of hydrothermal fluids caused alkaline minerals [12,47], mostly small deposits of shortite and reedmergnerite, to form at the basin edges. The sequence of lamina combinations in this stage was similar to the transitional stage of salinization, with FQL-SL and FQL-DOL forming at the edges of the basin and silicates precipitating to form the DOL-CL combination towards the center of the basin as a result of the decreasing pH.
5. The late stage of salinization corresponded to the late P_1f_2 deposition and the early P_1f_3 deposition and occurred in a shallow–semideep lacustrine environment. The climate was semiarid to semihumid, with rising lake levels and desalinated water. Alkaline minerals gradually disappeared in the weakly oxidizing–weakly reducing environment. In this period, the FQL-DOL combination was well developed, with little development of alkaline minerals.

6. Conclusions

Using slice identification, X-ray diffraction, XRF, scanning electron microscopy, nitrogen adsorption, and nano-CT, etc., the characteristics and origins of millimeter-scale laminae in the alkaline lacustrine strata of the P_1f_2 were investigated. The following conclusion are drawn:

There are five types of laminae in the P_1f_2, which form in four distinct combinations. The pore systems are predominantly composed of intercrystalline pores, intragranular pores, and dissolution pores of feldspar and dolomite, accompanied by imporous alkaline mineral particles. FQL and RL show distinct superiority in reservoir characteristics and oil-bearing properties. There is a marked positive correlation between porosity and TOC content but a negative correlation between lamina density and TOC content.

Single and mixed sources make up the material sources of the alkaline lacustrine shale series in the Junggar Basin. The FQL-DOL combination developed in single-terrestrial-source still water deposition and hybrid-source still water deposition. The FQL-RL combination and FQL-SL combination developed in single-terrestrial-source still water deposition and hybrid-source still water deposition. The DOL-CL combination developed in hybrid-source still water deposition and single-intrasource deposition.

The P_1f_2 has experienced five sedimentary evolution stages, with various combinations of salinization/desalinization, hydrothermal fluid influx, and environment changes. The initial and transitional stages of salinization were dominated by evaporative salinization, which formed Mg and Ca carbonates, shortite, and chert deposits; the FQL-DOL and FQL-SL combinations developed at the edges of the basin; and FQL-DOL-CL developed towards the basin center. In the high-level salinization stage, salinity reached its peak and alkaline mineral deposits developed under the action of hydrothermal fluids, primarily developing FQL-SL-RL. In the late recession stage, desalination occurred, and the sedi-

mentary characteristics reverted, becoming similar to the initial and transitional stages of salinization. In this period, FQL-SL and FQL-DOL developed at the edges of the basin and FQL-DOL-CL formed towards the center of the basin.

Author Contributions: Conceptualization, M.L. and S.W.; methodology, S.W.; software, M.L.; validation, P.W., Y.C. and S.Z.; formal analysis, M.L.; investigation, M.L.; resources, M.L.; data curation, M.L.; writing—original draft preparation, M.L.; writing—review and editing, M.L.; visualization, M.L.; supervision, S.H.; project administration, S.H.; funding acquisition, R.Z. All authors have read and agreed to the published version of the manuscript.

Funding: This research was funded by a National Natural Science Foundation of China (Grant No.42090025) and Major Science and Technology Project of China National Petroleum Corporation (Grant No. 2019E-2601).

Data Availability Statement: The data presented in this study are available on request from the corresponding author. The data are not publicly available due to privacy.

Acknowledgments: The authors would like to thank the Research Institute of Petroleum Exploration and Development (RIPED), China National Petroleum Corporation (CNPC), Beijing, China, for their help in our research. We appreciate the discussions and comments from all of the editors and anonymous reviewers.

Conflicts of Interest: Authors Songtao Wu, Rukai Zhu, Suyun Hu, Yi Cai and Surong Zhang were employed by the China National Petroleum Corporation (CNPC). The remaining authors declare that the research was conducted in the absence of any commercial or financial relationships that could be construed as a potential conflict of interest.

References

1. Javadpour, F.; Fisher, D.; Unsworth, M. Nanoscale gas flow in shale gas sediments. *J. Can. Pet. Technol.* **2007**, *46*, 55–61. [CrossRef]
2. Chalmers, G.R.; Bustin, R.M.; Power, I.M. Characterization of gas shale pore systems by porosimetry, pycnometry, surface area, and field emission scanning electron microscopy/transmission electron microscopy image analyses: Examples from the Barnett, Woodford, Haynesville, Marcellus, and Doig units. *AAPG Bull.* **2012**, *96*, 1099–1119.
3. Du, J.H.; Hu, S.Y.; Pang, Z.L.; Lin, S.H.; Hou, L.H.; Zhu, R.K. The types, potentials and prospects of continental shale oil in China. *China Pet. Explor.* **2019**, *24*, 560–568.
4. Hu, S.Y.; Li, J.Z.; Wang, T.S.; Wang, Z.C.; Yang, T.; Li, X.; Hou, L.H.; Yuan, X.J.; Zhu, R.K.; Bai, B.; et al. CNPC oil and gas resource potential and exploration target selection. *Pet. Geol. Exp.* **2020**, *42*, 813–823.
5. Lin, S.H.; Yuan, X.J.; Yang, Z. Comparative study on lacustrine shale and mudstone and its significance: A case from the 7th member of Yanchang Formation in the Ordos Basin. *Oil Gas Geol.* **2017**, *38*, 518–523.
6. Zhao, X.Z.; Zhou, L.H.; Pu, X.G.; Jin, F.M.; Shi, Z.N.; Xiao, D.Q.; Han, W.Z.; Jiang, W.Y.; Zhang, W.; Wang, H. Favorable formation conditions and enrichment characteristics of lacustrine facies shale oil in faulted lake basin: A case study of Member 2 of Kongdian Formation in Cangdong sag, Bohai Bay Basin. *Acta Pet. Sin.* **2019**, *40*, 1013–1029.
7. Jiang, Y.Q.; Wen, H.G.; Qi, L.Q.; Zhang, X.X.; Li, Y. Salt minerals and their genesis of the Permian Fengcheng Formation in Urho area, Junggar Basin. *J. Mineral. Petrol.* **2012**, *32*, 105–114.
8. Li, W.; Zhang, Y.Y.; Ni, M.J.; Tang, W.B. Genesis of alkaline lacustrine deposits in the Lower Permian Fengcheng Formation of the Mahu Sag, northwestern Junggar Basin: Insights from a comparison with the worldwide alkaline lacustrine deposits. *Acta Geol. Sin.* **2020**, *94*, 1839–1852.
9. Gong, B.S.; Wen, H.G.; Li, C.L.; Wang, L.; Zheng, R.C.; Qi, L.Q. Sedimentary environment of Fengcheng Formation in Urho area, Junggar Basin. *Lithol. Reserv.* **2014**, *26*, 59–66.
10. Zhao, Y.; Guo, P.; Lu, Z.Y.; Zheng, R.C.; Chang, H.L.; Wang, G.Z.; Wei, Y.; Wen, H.G. Genesis of Reedmergnerite in the Lower Permian Fengcheng Formation of the Junggar Basin, NE China. *Acta Sedimentol. Sin.* **2020**, *38*, 966–979.
11. Wang, L.B.; Hou, G.F.; Bian, B.L.; Li, Y.Z.; Dou, Y.; You, X.C.; Guo, H.J.; Xu, Y.; Zou, Z.W. The role of modern alkaline lakes in explaining the sedimentary environment of the Fengcheng Formation, Mahu Sag. *Acta Sedimento Log. Sin.* **2020**, *38*, 911–922.
12. Yu, Z.K.; Ding, J.G.; Feng, Z.W.; Jiang, L.Q.; Li, H.L.; Chang, X.B.; Zong, H.; Liang, J.W. Analysis on alkaline diagenesis of the Permian Fengcheng Formation in Mahu Sag, Junggar Basin. *Unconv. Oil Gas* **2021**, *8*, 24–32.
13. Li, C.Z.; Guo, P.; Ke, X.Q.; Ma, Y. Genesis of high-quality source rocks in volcano-related alkaline lakes and implications for the exploration and development of shale oil and gas. *Oil Gas Geol.* **2021**, *42*, 1423–1434.
14. O'Brien, N.R. Shale Lamination and Sedimentary Processes. *Geol. Soc. Lond. Spec. Publ.* **1996**, *116*, 23–36. [CrossRef]
15. Campbell, C.V. Lamina, laminaset, bed and bedset. *Sedimentology* **1967**, *8*, 7–26. [CrossRef]
16. Ingram, R.L. Terminology for the thickness of stratification and parting units in sedimentary rocks. *GSA Bull.* **1954**, *65*, 937–938. [CrossRef]

17. Kuroda, J.; Ohkouchi, N.; Ishii, T.; Tokuyama, H.; Taira, A. Lamina-scale analysis of sedimentary components in Cretaceous black shales by chemical compositional mapping: Implications for paleoenvironmental changes during the Oceanic Anoxic Events. *Geochim. Et Cosmochim. Acta* **2005**, *69*, 1479–1494. [CrossRef]
18. Shi, Z.S.; Qiu, Z.; Dong, D.Z.; Lu, B.; Liang, P.P.; Zhang, M.Q. Laminae characteristics of gas-bearing shale fine-grained sediment of the Silurian Longmaxi Formation of Well Wuxi 2 in Sichuan Basin, SW China. *Pet. Explor. Dev.* **2018**, *45*, 339–348. [CrossRef]
19. Wang, C.; Zhang, B.Q.; Hu, Q.H.; Shu, Z.G.; Sun, M.D.; Bao, H.Y. Laminae characteristics and influence on shale gas reservoir quality of lower Silurian Longmaxi Formation in the Jiaoshiba area of the Sichuan Basin, China. *Mar. Pet. Geol.* **2019**, *109*, 839–851. [CrossRef]
20. Li, M.Y.; Wu, S.T.; Hu, S.Y.; Zhu, R.K.; Meng, S.W.; Yang, J.R. Lamination texture and its effects on reservoir and geochemical properties of the Palaeogene Kongdian Formation in the Cangdong Sag, Bohai Bay Basin, China. *Minerals* **2021**, *11*, 1360. [CrossRef]
21. Bahk, J.J.; Chough, S.K.; Han, S.J. Origins and Paler ceanographic Significance of Laminated Muds from the Ulleung Basin, East Sea (Sea of Japan). *Mar. Geol.* **2000**, *162*, 459–477. [CrossRef]
22. Caplan, M.L.; Bustin, R.M. Palaeoenvironmental and Palaeoceanographic Controls on Black, Laminated Mudrock Deposition: Example from Devoniar Carboniferous Strata, Alberta, Canada. *Sediment. Geol.* **2001**, *145*, 45–72. [CrossRef]
23. Leclair, S.F.; Arnott, R.W.C.; Parallel, L. Lamination Formed by High-Density Turbidity Currents. *J. Sediment. Res.* **2005**, *75*, 1–5. [CrossRef]
24. Zolitschka, B.; Francus, P.; Ojala, A.E.K.; Schimmelmann, A. Varves in lake sediments-a review. *Quat. Sci. Rev.* **2015**, *117*, 1–41. [CrossRef]
25. Schieber, J. Experimental testing of the transport-durability of shale lithics and its implications for interpreting the rock record. *Sediment. Geol.* **2016**, *331*, 162–169. [CrossRef]
26. Yan, J.H.; Deng, Y.; Pu, X.G.; Zhou, L.H.; Chen, S.Y.; Jiao, Y.X. Characteristics and controlling factors of fine-grained mixed sedimentary rocks from the 2nd Member of Kongdian Formation in the Cangdong Sag, Bohai Bay Basin. *Oil Gas Geol.* **2017**, *38*, 98–109.
27. Liu, G.H.; Huang, Z.L.; Jiang, Z.X.; Chen, J.F.; Chen, C.C.; Gao, X.Y. The characteristic and reservoir significance of lamina in shale from Yanchang Formation of Ordos Basin. *Nat. Gas Geosci.* **2015**, *26*, 408–417.
28. Ilgen, A.G.; Heath, J.E.; Akkutlu, I.Y.; Bryndzia, L.T.; Cole, D.R.; Kharaka, Y.K.; Kneafsey, T.J.; Milliken, K.L.; Pyrak-Nolte, L.J.; Suarez-Rivera, R. Shales at all scales: Exploring coupled processes in mudrocks. *Earth Sci. Rev.* **2017**, *166*, 132–152. [CrossRef]
29. Shi, Z.S.; Dong, D.Z.; Wang, H.Y.; Sun, S.S.; Wu, J. Reservoir characteristics and genetic mechanisms of gas-bearing shales with different laminae and laminae combinations: A case study of Member 1 of the Lower Silurian Longmaxi shale in Sichuan Basin, SW China. *Pet. Explor. Dev.* **2020**, *47*, 829–840. [CrossRef]
30. Ablimit, I.; Tang, Y.; Cao, J.; Chen, G.; Chen, J.; Tao, K. Accumulation mechanism and enrichment rules of the continuous hydrocarbon plays in the lower Triassic baikouquan Formation of the mahu Sag, Junggar Basin. *Nat. Gas Geosci* **2016**, *27*, 241–250.
31. Song, Y.; Zhou, L.; Guo, X.G.; Chang, Q.S.; Wang, X.T. Characteristics and occurrence of lacustrine dolomitic tight-oil reservoir in the Middle Permian Lucaogou Formation, Jimusa er Sag, southeastern Junggar Basin. *Acta Petrol. Sin.* **2017**, *33*, 1159–1170.
32. Wang, Y.; Chen, S.Y.; Zhang, G.L.; Zhang, K.H.; Lin, H.X.; Liang, H.Y.; Wang, Y.X.; Li, X. Classification of mixosedimentite and sedimentary facies characteristics of mixed sedimentary facies belt in saline lacustrine basin: Taking examples as the Lucaogou Formation in the south of Junggar Basin and the Taerlang Formation in the northeast of Tuha Basin. *Acta Pet. Sin.* **2017**, *38*, 1021–1035.
33. Carroll, A.R.; Liang, Y.H.; Graham, S.A.; Xiao, X.C.; Hendrix, M.S.; Chu, J.C. McKnight Junggar basin, northwest China: Trapped late paleozoic ocean. *Tectonophysics* **1990**, *181*, 1–14. [CrossRef]
34. Chen, S.P.; Zhang, Y.W.; Tang, L.J. Evolution of Junggar late Carboniferous-Permian foreland basin. *J. China Univ. Pet.* **2001**, *25*, 11–15.
35. Wu, K.Y.; Zha, M.; Wang, X.L.; Qu, J.X.; Chen, X. Further researches on the tectonic evolution and dynamic setting of the Junggar Basin. *Acta Geosci. Sin.* **2005**, *26*, 217–222.
36. Feng, Q.; Liu, Y.Q.; Hao, J.R. The source rock and its palaeo-environment of Lucaogou Formation, Permian in Santanghu Basin. *Acta Sedimentol. Sin.* **2004**, *22*, 513–517.
37. Zhi, D.M.; Song, Y.; He, W.J.; Jia, X.Y.; Zou, Y.; Huang, L.L. Geological characteristics, resource potential and exploration direction of Middle Lower Permian shale oil in Junggar Basin. *Xinjiang Pet. Geol.* **2019**, *40*, 389–401.
38. Tang, Y.; Zheng, M.L.; Wang, X.T.; Wang, T.; Xie, Z.B.; Qin, Z. Sedimentary paleoenvironment of source rocks of Fengcheng Formation in Mahu Sag of Jungar Basin. *Nat. Gas Geosci.* **2022**, *11*, 664.
39. Liu, D.G.; Zhou, L.; Li, S.H.; Ma, W.Y.; Guo, W.J. Characteristics of Source Rocks and Hydrocarbon Generation Models of Fengcheng Formation in Mahu Sag. *Acta Sedimentol. Sin.* **2020**, *38*, 946–955.
40. *GB/T 19145-2003*; Determination of Total Organic Carbon in Sedimentary Rock. General Administration of Quality Supervision, Inspection and Quarantine of the People's Republic of China: Beijing, China, 2022.
41. *GB/T 18602-2001*; Rock Pyrolysis Analysis. General Administration of Quality Supervision, Inspection and Quarantine of the People's Republic of China: Beijing, China, 2013.
42. *SY/T7410.1-2018*; 3D Pore Structure Characterization of Rocks. National Energy Administration: Beijing, China, 2018.

43. Tang, Y.; Lu, Z.X.; He, W.J.; Qing, Y.H.; Li, X.; Song, X.Z.; Yang, S.; Cao, Q.M.; Qian, Y.X.; Zhao, X.M. Origin of dolomites in the Permian dolomitic reservoirs of Fengcheng Formation in Mahu Sag, Junggar Basin, NW China. *Pet. Explor. Dev.* **2023**, *50*, 38–50. [CrossRef]
44. Zhang, Z.J.; Yuan, X.J.; Wang, M.S.; Zhou, C.M.; Tang, Y.; Chen, X.Y.; Lin, M.J.; Cheng, D.W. Alkaline-lacustrine deposition and Paleoenvironmental evolution in Permian Fengcheng Formation at the Mahu Sag, Junggar Basin, NW China. *Pet. Explor. Dev.* **2018**, *45*, 972–984. [CrossRef]
45. Wang, K.M.; Luo, S.S. Geochemical characteristics and environmental significance of Gaoyuzhuang and Yangzhuang Formations in Yanshan region. *Bull. Mineral. Petrol. Geochem.* **2009**, *28*, 356–364.
46. Jiang, Z.F.; Jiang, M.Y.; Chen, H.L.; Liu, L.S.; Wang, X.Y.; Bian, B.L.; Li, N. Thermal and Paleoenvironment Evolution of the Fengcheng Formation of Permian in Mahu Depression, Junggar Basin. *Geoscience* **2022**, *36*, 1118–1130.
47. Yu, K.H.; Cao, Y.C.; Qiu, L.W.; Sun, P.P.; Yang, Y.Q.; Qu, C.S.; Wan, M. Characteristics of alkaline layer cycles and origin of the lower Permian Fengcheng formation in Mahu sag, Junggar Basin. *J. Palaeogeogr.* **2016**, *18*, 1012–1029.
48. Lazar, O.R.; Bohacs, K.M.; Macquaker, J. Capturing Key Attributes of Fine-Grained Sedimentary Rocks in Outcrops, Cores, and Thin Sections: Nomenclature and Description Guidelines. *J. Sediment. Res.* **2015**, *85*, 230–246. [CrossRef]
49. Dittrich, M.; Obst, M. Are picoplankton responsible for calcite precipitation in lakes. *Ambio* **2004**, *33*, 559–564. [CrossRef]
50. Zhang, J.G.; Jiang, Z.X.; Liu, P.; Kong, X.X.; Ge, Y.J. Deposition mechanism and geological assessment of continental ultrafine-grained shale oil reservoirs. *Acta Pet. Sin.* **2022**, *43*, 234–249.
51. Wang, S.Z.; Zhang, K.H.; Jin, Q. The genetic types of crude oils and the petroleum geological significance of the Fengcheng Formation. *Nat. Gas Geosci.* **2014**, *25*, 595–602.